A HfS$_2$-based photoelectronic synaptic transistor with tunable synaptic plasticity for emotional memory

Qiangfei Wang [a], Ruiqi Jiang [a], Zhaotan Gao [a], Menghan Deng [a], Junhui Chen [a], Liangqing Zhu [a], Liyan Shang [a], Yawei Li [a], Dirk Fuchs [b], Jinzhong Zhang [a,*], Zhigao Hu [a,c]

[a] Technical Center for Multifunctional Magneto-Optical Spectroscopy (Shanghai), Engineering Research Center of Nanophotonics & Advanced Instrument (Ministry of Education), Department of Physics, School of Physics and Electronics Science, East China Normal University, Shanghai 200241, China
[b] Karlsruhe Institute of Technology, Institute for Quantum Materials and Technologies, 76021, Karlsruhe, Germany
[c] Collaborative Innovation Center of Extreme Optics, Shanxi University, Taiyuan, Shanxi 030006, China

A R T I C L E   I N F O

A B S T R A C T

Neuromorphic computing has attracted great attention to mimic the human brain functions of perception, learning, and memory, which is considered to overcome the "von Neumann bottleneck". Here, we developed a HfS$_2$-based photoelectronic field effect transistor with a tunable synaptic plasticity. By modulating the gate voltages, the paired-pulse plasticity undergoes a transition between paired-pulse facilitation (PPF = 128%) and paired-pulse depression (PPD = 89%) due to the charge-trapping effect under a pulsed light ($\lambda = 405$ nm). In a further step, five emotion valences and emotion-related learning and memories are successfully mimicked based on the various artificial synaptic metaplasticity of the HfS$_2$-based synaptic devices. This work provides an alternative approach to modulate the synaptic plasticity of artificial synaptic transistors for emotional memory and a new strategy to improve brain-like simulations of neuromorphic computing.

1. Introduction

Human brain can recognize information from external stimuli through a biological sensory system. The central and peripheral nervous system works together to recognize external information, to make decisions, and to control bodily functions [1,2]. Unlike the "von Neumann" architecture, the human brain uses the same interval for storage and computation. The operations are asynchronous, energy efficient, massively parallel, and fault tolerant [3 5]. Inspired by the highly connected and extremely energy efficient neural networks of the human brain, neuromorphic computing, as a new paradigm, has implications for advanced cognition, reasoning, and learning as well as traditional data processing and storage [6 8]. Recently, the construction of artificial nervous systems at the device level has become an important branch in the field of artificial intelligence [9 11].

As an important structure, synapses connect billions of neuronal cells in the human brain [12]. Simulation of biological functions through synaptic devices is an important part of the brain like engineering. By regulating synaptic plasticity, information can be processed and stored at the same time. The synaptic plasticity includes short term synaptic plasticity (STP), long term synaptic plasticity (LTP), paired pulse facilitation (PPF), paired pulse depression (PPD), *etc* [13]. STP and LTP have been implicated in short and long term learning and

memory in the human brain. Paired pulse plasticity (PPF and PPD) is the basis of various synaptic functions. The investigation of paired pulse plasticity is helpful to expand the synaptic functions of devices and improve the degree of simulation. Lin et al. demonstrated that PPF behavior is negatively correlated with pulse interval in a two dimensional (2D) layered InSe based photonic synaptic device, which could mimic age related synaptic plasticity in the human brain [14]. Wang et al. reported a CsPbBr$_3$/h BN/Graphene based synaptic device with a high PPF index (196%) under the same wavelength of pulsed light, which could be applied for artificial visual perception systems [15]. Hu et al. implemented a 2D layered HfS$_2$ based artificial optoelectronic synapse for recognition of handwritten numbers with an accuracy of about 91.5% and a low energy consumption of 0.2 pJ per spike [16]. However, there are still some challenges which have to be overcome for 2D layered material based artificial synaptic devices [17]. Firstly, most 2D materials are easily attacked by air. Oxidation and hydrolysis cannot be completely avoided under the vacuum condition. Secondly, paired pulse plasticity under a pulsed light always exhibits a facilitation behavior without a depression [18,19]. Thirdly, emotions could affect the learning and forgetting behaviors, [20,21] while the physical mechanism of artificial synaptic devices for emotional memory is not clear. This needs to be investigated further in detail.

As a type of transition metal dichalcogenides, layered semiconductor HfS_2 exhibits excellent electrical and optical properties. It has an indirect band gap of 1.2 eV, an ultra sensitive light response, and a super high theoretical acoustic phonon limited mobility of 1800 3500 $cm^2V^{-1}s^{-1}$ [22,23]. Similar to other transition metal dichalcogenides (TMDs), layered HfS_2 exhibits different properties with increasing the number of layers. For examples, Nie et al. reported that multilayer TMD FETs possess higher current carrying capacities and mobility than those of monolayer TMD devices [24]. Xu et al. demonstrate that the 7 12 nm thick HfS_2 based FETs exhibit the maximal mobility and on/off ratio [25]. In this work, 7 12 nm thick HfS_2 nanosheets were transferred to the 280 nm thick SiO_2/Si substrates. To ensure the thickness of HfS_2 sheets is uniform, the optical microscope and an atomic force microscope (AFM) system are used to determine the thickness. In a further step, a HfS_2 based synaptic transistor was designed and fabricated, which was covered with indium (In) to improve the stability [26,27]. There is a transition between PPF and PPD under the same wavelength of pulsed light ($\lambda = 405$ nm) due to the good gate control of the field effect transistors (FETs) and the HfS_2/SiO_2 interfacial charge trapping effect. The tunable paired pulse synaptic plasticity of the HfS_2 based synaptic device mainly includes stabilization, multi level facilitation and depression. Moreover, emotion related synaptic metaplasticity is simulated by modulating the charge trapping/detrapping effect under different light pulse frequencies and gate voltages (V_{GS}). Finally, thirty emotional states are defined by the synaptic weight index, and the emotion related learning and memory processes are investigated in detail for artificial emotional memories.

2. Material and methods

2.1. Device fabrication

HfS_2 sheets were mechanically exfoliated from the HfS_2 crystals (Sixcarbon Tech Shenzhen) onto polydimethylsiloxane (PDMS) films, and then transferred to the 280 nm thick SiO_2/Si substrates. A 5 nm thick indium (In) layer was deposited on the HfS_2 sheets at a rate of 0.1 Å/s by a thermal evaporation machine with a deposit current of 75 A under high vacuum (10^{-6} Torr). The source and drain electrodes (Ni/Au, 2/50 nm) were fabricated on the transferred HfS_2 sheets by thermal evaporation using a shadow mask.

2.2. Characterization

The morphology and thickness of HfS_2 sheets on the SiO_2/Si were measured using an optical microscope and an atomic force microscope (AFM, Dimension Icon, Bruker). Raman spectra were recorded by a Raman microscope (Jobin Yvon LabRAM HR Evolution, HORIBA) with an excitation laser of 532 nm. The electrical and optoelectronic characteristics of the HfS_2 based devices were probed with the Keithley 4200 SCS semiconductor parameter analyzer under high vacuum (10^{-6} Torr) at room temperature. All the electronic and optoelectronic measurements in the probe station were carried out under dark conditions, and only exposed to the target light sources. For the optoelectronic measurements, commercial light emitting diodes with wavelengths of 405, 520, and 638 nm (Thorlabs, Inc.) were employed. Light pulses with tunable power intensity, pulse width, and frequency were controlled using a laser diode/temperature controller.

3. Results and discussion

3.1. Structure and electrical/optical performance of HfS_2 based transistors

Fig. 1a illustrates the architecture of a HfS_2 based transistor to mimic photoelectric synapses. Note that a 5 nm indium layer was deposited by thermal evaporation to protect the device from oxidation.

The deposition of In could reduce the damage of channel materials during evaporation since In has a lower melting point (156 °C), compared with Al (660 °C) and Hf (2227 °C). Fig. 1b shows the optical microscope image of a HfS_2 based transistor. The channel length and channel width of the device are about 14 μm and 40 μm, respectively. The AFM image suggests that the HfS_2 sheet has a clean surface. The corresponding height profile reveals that the thickness is about 9.6 nm (cf. Figure S1a in the Supporting Information), which is expected to show brilliant performance [28]. In Fig. 1c, there are two peaks nearby 260 and 338 cm^{-1} in the Raman spectra of HfS_2 sheets, which are assigned to the first order Raman active modes E_g and A_{1g}, respectively [25]. Note that the Raman peak ($\star$) nearby 302 cm^{-1} comes from the two transverse acoustic phonons (2TA) of the Si substrate (cf. Figure S1b) [29].

Fig. 1d shows the output characteristics at different gate source voltages (V_{GS}) from -80 V to $+80$ V, which exhibits an Ohmic contact for the HfS_2 based FETs. In Figs. 1e and S1c, the transfer characteristic curves at different drain source voltage (V_{DS}) reveal a n type feature of the HfS_2 channel with a high on/off ratio of about 10^5. It should be emphasized that there is a tiny hysteresis in the transfer characteristic curves due to the charge trapping effect caused by the Si O dangling bonds on the SiO_2 surface [22]. The HfS_2 FETs show decent environmental stability, which maintains the normal electrical performance for more than seven weeks (cf. Figure S1d). In addition, the HfS_2 based FETs have a high repetition rate according to the transfer characteristic curves, as shown in Figure S2a. However, there are still some variations between different devices, which could be attributed to the various thickness of HfS_2 sheets. Fig. 1e shows the transfer characteristics of the HfS_2 FETs under various power densities of the 405 nm laser at V_{DS} = 0.1 V. The threshold voltage (V_{th}) shifts toward the negative voltage side as the light power density increases from 0 to 58 mW/cm^2 since the photocarrier concentration increases. The device responsivity (R) as a function of light power density is defined by the formula:[30] $R = I_{ph}/(P_{in} \cdot S)$, where $I_{ph} = I_{light}$ I_{dark}, P_{in} is the laser power density, and S is the active area of the phototransistor. Fig. 1f suggests that the responsivity decreases and then tends to be saturated with increasing the power density. It has a maximum value of about 23 A/W at $P_{in} = 1.8 \, mW/cm^2$. As the laser power density increases, the excited photocarriers (i.e., I_{ph}) in the channel increases, as shown in the inset of Fig. 1f.

3.2. Mechanism of the gate regulated synaptic plasticity

The charge trapping effect is a key mechanism for memory behavior in photosynapse transistors since it affects the synaptic plasticity [31]. To further confirm the origin of the trapping event, a layered insulator (h BN) with free dangling bonds was inserted into the HfS_2/SiO_2 interface (cf. Figure S2b). For the devices with the SiO_2/h BN/HfS_2 structure, the hysteresis is reduced compared with that of HfS_2/SiO_2 structure. It indicates that the introduction of h BN prevents carriers from being trapped. Therefore, the acceptor like charge trapping behavior in the present devices originates from the dangling Si O bonds at the SiO_2 surface. Fortunately, the captured electrons in the artificial synaptic transistors could be regulated by V_{GS} [32]. To better understand the operation mechanism, the band structure and carrier behavior of the HfS_2/SiO_2 based synaptic FETs at the positive and negative V_{GS} are illustrated in Figs. 2a and 2b, respectively. In particular, the bands of HfS_2 bend downward when a positive V_{GS} is applied. The carriers accumulate at the HfS_2/SiO_2 interface and are captured by defect states on the SiO_2 surface, which reduces the output current (cf. Figure S3a). This suggests that the output current decays with the time at $V_{GS} = 80$ V. In contrast, when a negative V_{GS} is applied, the trapped carriers are released back into the channel, resulting in an increase of the output current (cf. Figure S3b). Moreover, Figs. 2c and 2d show the energy band diagrams and carrier behavior during/after illumination at $V_{GS} = 0$ V. When light is applied, a large number of photocarriers will be generated in the channel, resulting in a rapid increase of current in a
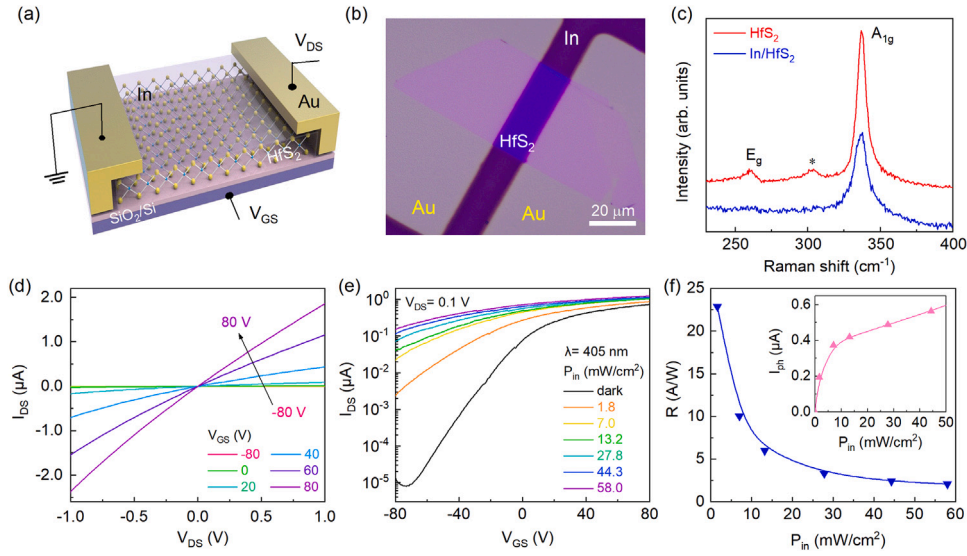
Fig. 1. (a) Schematic illustration of a HfS$_2$-based FET, packaged with In as a passivation layer. (b) An optical image of a HfS$_2$-based FET covered with a 5 nm-thick In layer. (c) Raman spectra of the In/HfS$_2$ and HfS$_2$ sheets on SiO$_2$/Si substrates used in the devices and the corresponding assignment of the Raman peaks. The Raman peak (⋆) nearby 302 cm^{-1} comes from Si substrates. (d) Output characteristic curves of a HfS$_2$-based FET in the dark at various V$_{GS}$. (e) Transfer characteristic curves at different laser power densities. (f) Responsivity and I$_{ph}$ (inset) of the HfS$_2$-based optoelectronic device as a function of laser power density.
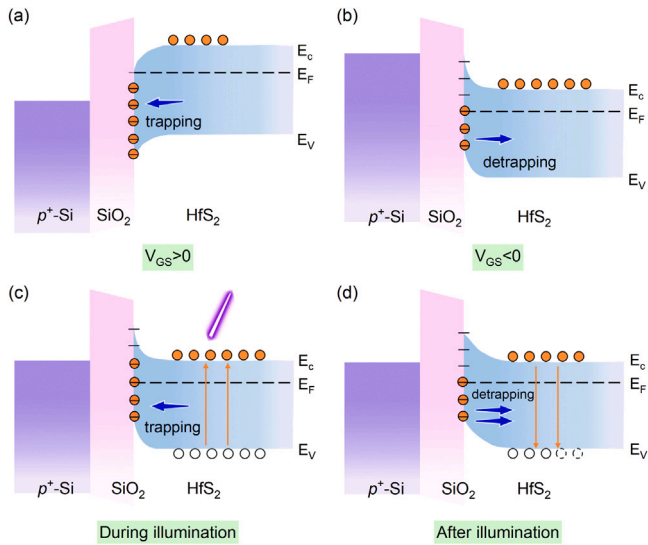
Fig. 2. Energy band diagrams of the HfS$_2$/SiO$_2$/p^+-Si architecture. (a) The carrier capture process under positive V$_{GS}$. (b) The carrier release process under negative V$_{GS}$. (c) The carrier capture process during illumination. (d) The carrier release process after illumination.

short time. At the same time, the defect states at the HfS$_2$/SiO$_2$ interface will capture a fraction of photocarriers. When light is removed, the combination of electrons and holes causes the decrease of post synaptic current (PSC). However, the interface trap can release a small fraction of electrons to the channel and the output current will not drop back to the initial state [33].

3.3. Tunable synaptic plasticity of HfS$_2$ based transistors

In neurobiology, two adjacent neurons are connected by synapses, and signals are transmitted by chemicals. The presynaptic neuron releases neurotransmitters, which are then picked up by receptors on the postsynaptic neuron [34]. Similar to biological synapses, [35] the light stimulation can be regarded as pre spike and the channel as post spike as illustrated in Fig. 3a. The post synaptic current (PSC) of a

HfS$_2$ synaptic device is triggered by a single light pulse (405, 520, and 633 nm) with a fixed power density of 44.3 mW/cm^2 and a pulse width of 0.5 s. It reveals that the PSC triggered by the 405 nm pulsed light is the largest one (cf. Figure S4). In order to achieve obvious synaptic functions, the 405 nm laser is performed in the following experiments. Fig. 3b shows the time dependent PSC by applying a single light pulse with the different pulse widths from 0.1 s to 1.2 s. The PSC increases sharply during illumination and decays after illumination. Note that PSC does not return to the initial state due to the charge trapping effect. The PSC increases with increasing the pulse width, which is consistent with the pulse time dependent plasticity [36]. In Figure S5, the PSC decay curves are simulated by a simplified Kohlrausch law: [37] $I = I_0 + I_1 \times \exp[-(t/\tau)^\beta]$. For the case of the laser pulse width of 0.5 s, the extracted stretch index (β) is 0.278 ± 0.001 and the retention time (τ) is about 212 ± 3 ms. This means that the feature time of the carrier migration is about 212 ms. The single pulse index is obtained by the formula: [22] $\Delta PSC/PSC = (A - A_0)/A \times 100\%$. Where A and A$_0$ are the amplitudes of the PSC when lighting and the initial state before lighting, respectively. In the inset of Fig. 3b, the single pulse index increases with the pulse width and tends to be saturated at about 0.3 s. Figs. 3c and S6 indicate that the PSC has a similar behavior by applying a single light pulse with various amplitudes from 1.8 to 44.3 mW/cm^2 and a fixed pulse width of 0.5 s, which verifies the pulse amplitude dependence of the synapse plasticity. The inset of Fig. 3c depicts that the single pulse index increases with the pulse amplitude and tends to be saturated under a high light power density above 10 mW/cm^2.

Paired pulse synaptic plasticity (PPF and PPD) refers to the related change of the synaptic response after the first and second consecutive stimuli [38]. Usually, the paired pulse index is defined by the following formula: [39,40] PPF (PPD) index $= A_2/A_1 \times 100\%$, where A$_1$ and A$_2$ are the amplitudes of the first and second PSC, respectively. As shown in Figs. 3d, 3e and S7, a tunable paired pulse plasticity feature is demonstrated by applying negative and positive gate voltages. In particular, PPF behavior occurs at V$_{GS} = -80$ V according to the ratio of A$_2$/A$_1$ (128%). Interestingly, the paired pulse plasticity is reversed from PPF to PPD at V$_{GS} = +80$ V with a PPD index of about 89%. It should be emphasized that the PSC amplitudes (A$_1$ and A$_2$) are corrected with respect to the background current for positive gate voltages (cf. Figure S8). The paired pulse synaptic plasticity consists of three stages: first stimulation, intermediate relaxation, and second stimulation [15]. For the case of V$_{GS} = 0$ V, the PSC increases due
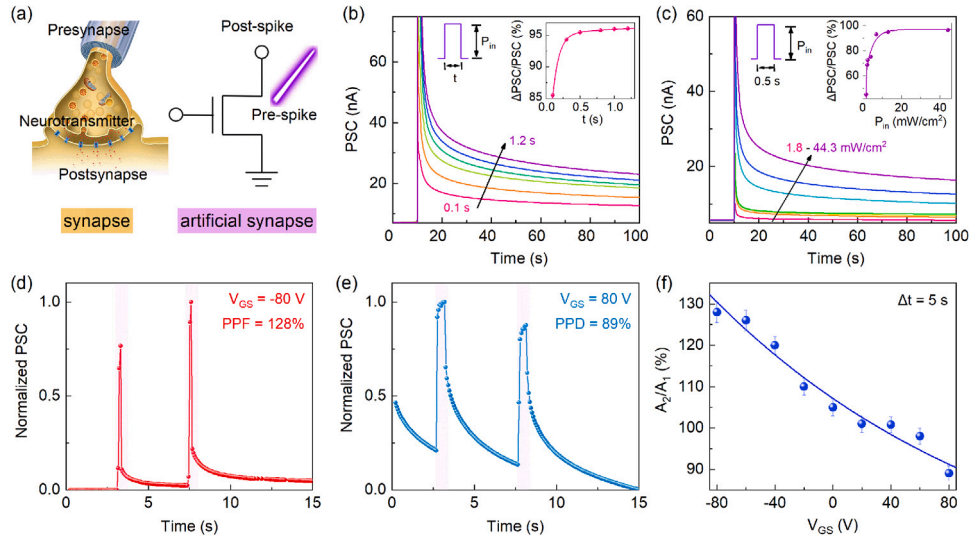
Fig. 3. (a) Schematic diagrams of a biological synapse and an artificial synapse based on the HfS$_2$-based FET. (b) PSC stimulated by a single light pulse with different laser pulse width from 0.1 to 1.2 s and a fixed power density of 44.3 mW/cm^2. Inset: The corresponding single pulse index (ΔPSC/PSC) as a function of light pulse width. (c) PSC stimulated by a single light pulse with different power densities from 1.8 to 44.3mW/cm^2 and a fixed duration time of 0.5 s. Inset: The corresponding single pulse index as a function of light power density. Normalized PSC stimulated by a pair of light pulses (power density: P$_{in}$ = 44.3 mW/cm^2, pulse interval: Δt = 5 s, and pulse width: t = 0.5 s) at the V$_{GS}$ of (d) −80 V and (e) 80 V. (f) The corresponding paired-pulse index (A$_2$/A$_1$) and the best-fitted curve as a function of V$_{GS}$ at a laser pulse interval of Δt = 5 s.

Table 1
Comparison of the key parameters of some typical optoelectronic synaptic devices.

| Active material	Size/thick. (μm^2/nm)	On/Off ratio	λ (nm)	Resp. (A/W)	Optical spike (PPF/PPD)	Refs.
HfS$_2$	14 × 40/9.6	>10^5	405	23	128%/89%	This work
HfS$_2$	5 × 18/20	>10^5	405	0.09	150%/–	[16]
HfS$_2$	3 × 10/9.8	~10^6	405	0.02	111%/–	[22]
HfS$_2$	–/11.1	~10^5	405	10^{-3}	140%/–	[26]
InSe	–	~10^7	405	–	210%/–	[14]
IZO	30 × 100/40	~10^5	470	4 × 10^{-3}	130%/–	[9]
CsPbBr$_3$	200 × 500/30	–	520	4	196%/–	[15]
Si/P3HT	25 × 500/100	–	375	8 × 10^{-5}	154%/–	[40]
			532	2.7 × 10^{-5}	–/54%	[40]
MAPbI$_3$	25 × 500/205	–	532	120	168%/–	[41]

to the presence of photogenic carriers during the first stimulus. In the intermediate relaxation stage, the combination of photogenerated electrons and holes leads to the PSC decline, which is the background current of the secondary stimulus. At the same time, the part of the photocarriers are captured in trapped states. When the second stimulus is applied, photocarriers are again accumulated over the background current, resulting in a larger current than that of the first stimulus. For the case of V$_{GS}$ > 0 V, the carriers move from the channel to the HfS$_2$/SiO$_2$ interface. The background current decays quickly due to the enhanced charge trapping effect. Therefore, the PSC stimulated by the second stimulus is weaker than that by the first stimulus. On the contrary, the charge trapping effect is attenuated and a part of the trapped carriers are released to the channel at V$_{GS}$ < 0 V. The second stimulus is stronger than the first stimulus since the background current increases. In Figs. 3f, the A$_2$/A$_1$ index decreases from 128% (PPF) to 89% (PPD) with increasing the gate voltage from −80 V to +80 V. This indicates that the present synaptic devices have a tunable paired pulse plasticity and the PPF/PPD transition occurs when the sign of gate voltage changes due to the enhancement or attenuation of charge trapping effect. In addition, the key parameters of different synapse devices are compared in Table 1. It is found that the present HfS$_2$ based artificial synapses have a high responsivity of 23 A/W, a good on/off ratio of about 10^5, and both optical spikes (PPF/PPD = 128%/89%) by applying the same pulsed light (λ = 405 nm) at various gate voltages.

Generally, PPF index decreases and PPD index increases monotonically with increasing the pulse interval [16,42]. Interestingly, in this work, PPF and PPD are positively and negatively correlated with the light pulse interval Δt, respectively (cf. Fig. 4a). At V$_{GS}$ = 0 V, the PPF index decreases with Δt since the photogenerated carriers have enough time to recombine, which induces a low background current for the second stimulus [43]. When the gate bias is 40 V or 80 V, the background current decreases with Δt due to the enhanced charge trapping effect. The index shows a negative correlation with Δt and reaches a minimum value of 89% at V$_{GS}$ = 80 V and Δt = 5 s. The trend is reversed at V$_{GS}$ = −40 V and −80 V, as shown in Fig. 4a. The PPF index shows a positive correlation with Δt, and it reaches a maximum value of 128% at V$_{GS}$ = −80 V and Δt = 5 s. The background current increases with increasing Δt due to the attenuated charge trapping effect (cf. Figure S9). When the pulse interval is small, few carriers are captured to make a lower second stimulus. When the pulse interval is long enough (Δt ≥ 2 s), there is a transition from PPF to PPD at V$_{GS}$ = 80 V. Note that the high gate voltage will decrease dramatically for the case of a thin high k dielectric oxidation layer in the synaptic transistors.

In a further step, the synaptic plasticity (STP and LTP) of the HfS$_2$ artificial devices is investigated by applying the pulsed light (P$_{in}$ = 44.3 mW/cm^2 and t = 0.5 s), as shown in Figs. 4b and S10. The captured carriers at the HfS$_2$/SiO$_2$ interface are released back to the conducting channel and the output current level increases by applying a negative gate voltage. Therefore, when light stimulation is applied to HfS$_2$ FETs, a large PSC can be obtained based on the increase of output current, leading to LTP. Fortunately, it can be reset to a lower conductivity state after applying a positive pulsed gate voltage. (cf. Figure S11) On the other hand, a small PSC can be obtained based on the decrease of output current under a positive gate voltage, leading
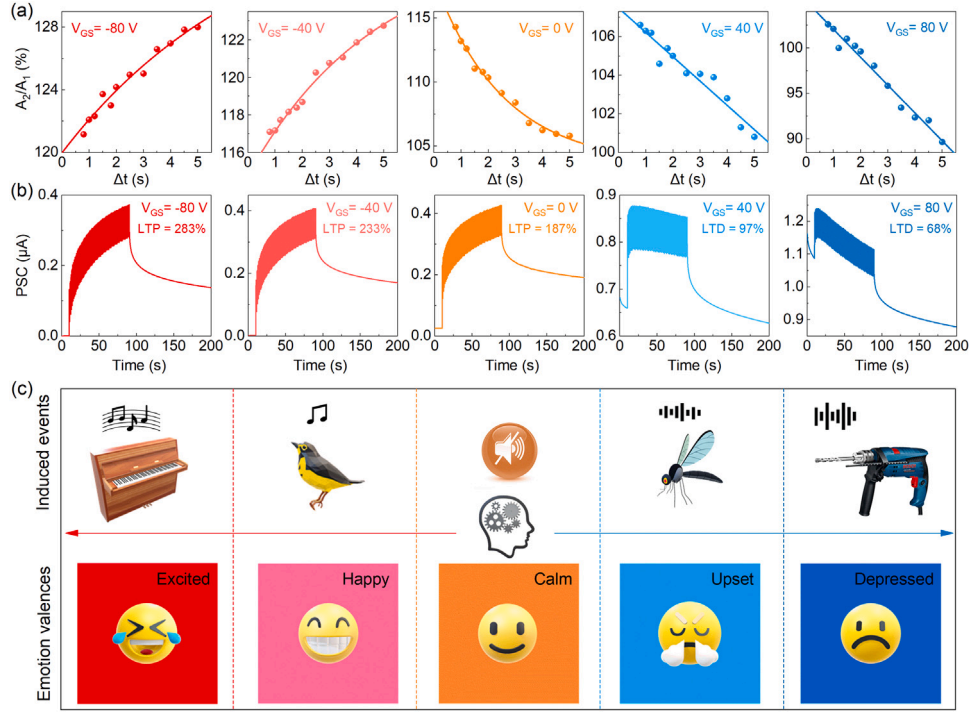
Fig. 4. (a) A_2/A_1 index as a function of light pulse interval Δt at $V_{GS} = -80$, -40, 0, $+40$, and $+80$ V. (b) PSC stimulated by light pulses (pulse number: 80, power density: 44.3 mW/cm^2, pulse width: 0.5 s, and pulse frequency: 1 Hz) at various V_{GS}. (c) The five kinds of induced events and the corresponding five emotional valences based on the tunable synaptic plasticity.

to LTD. Note that the synapse weight (W) is obtained based on the formula:[28] $W_n = A_n/A_1 \times 100\%$. Here A_1 and A_n are the amplitudes of the first and nth PSC, respectively. It reveals that the synaptic weight is enhanced by applying a negative gate voltage, while it is weakened by applying a positive gate bias. Particularly, the synaptic weight increases to the maximum (283%) at -80 V and decreases to the minimum (68%) at 80 V. It indicates that synaptic metaplasticity of the HfS$_2$ based synaptic transistors are realized by applying various V_{GS}.

In human sense, one perceives the world subjectively, and the perception could be influenced by the environment, resulting in different emotions [44]. In neurobiology, the learning and forgetting are affected by emotions under different induced events, which provides the support for imitating the memory processes of a person under different emotion states. In psychology, emotion is composed of the two dimensions (valence and arousal) according to the two dimensional theory of emotion. The emotional valence can be divided into positive, neutral, and negative emotion valences [45,46]. The synaptic weight could mimic different emotional valences in humans [47,48]. In this work, the phenomena of learning and forgetting can be affected by the synaptic weights of synaptic transistors at different gate voltages. Fig. 4c shows the five kinds of emotional valences under the corresponding induced events. Note that gate voltage corresponds to the induced emotional events. Particularly, $V_{GS} = 0$ V is used for neutral events, a negative V_{GS} for good induced events, and a positive V_{GS} for bad induced ones. When one is in a quiet environment, the emotional valence is calm (187%). One will be happy (233%) when hearing the chirping of a bird, and excited (283%) when hearing a song. On the contrary, one will become upset (97%) when hearing the sound from a mosquito, and depressed (68%) when hearing the noise from a drill. Therefore, the present synaptic transistors could be used to simulate emotions in different environments.

For the other dimensional emotion arousal, the high degree of emotions lead to high arousal and great mood swings [47,49]. Arousal emotions are further simulated by various light pulse frequencies, as shown in Figs. 5 and S12. The PSC at a light pulse frequency of 0.2 Hz decays quickly and reaches a low level of the biological synapses, which
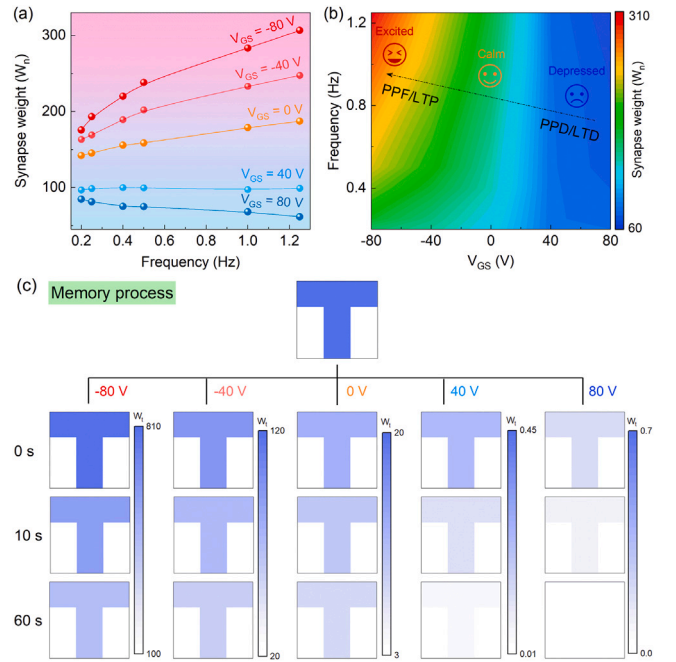
Fig. 5. (a) Synapse weight (W_n) as a function of laser pulse frequency at different V_{GS} from -80 V to $+80$ V. (b) A contour map of W_n as a function of laser pulse frequency and V_{GS} with an obvious inversion of states of emotion. (c) The memory process of the letter 'T' under the positive, neutral, and negative states of mood, which are denoted by $V_{GS} = -80$ V, -40 V, 0 V, 40 V, and 80 V, respectively.

simulates a STP like behavior. When the frequency increases to 1.25 Hz, the PSC reaches a high level after frequent stimulation. Fig. 5a suggests that the synaptic weight increases with the light pulse frequency at a positive V_{GS}, and decreases with the light pulse frequency at a negative

V_{GS}. The synapse weight (W_n) increases with increasing the frequency. It means that more frequent practice leads to an enhanced learning, which transfers from fast to slow reinforcement, eventually stabilizing to a long term memory. Different pulse frequencies could represent different degrees of arousal under the same emotional valence. There is a corresponding emotional state at the junction of V_{GS} (emotional valence) and frequency (emotional arousal). The range of V_{GS} is from −80 to 80 V, which contains five values. The pulse frequency ranges from 0.2 to 1.25 Hz, which contains six values. Therefore, thirty emotional states are defined. The A_n/A_1 index as a function of laser pulse frequency and V_{GS} is plotted in Fig. 5b, which corresponds to the two dimensional model diagram composed of emotional valence and arousal. Emotion is positively correlated with arousal under a positive emotional valence, while it is negatively correlated with arousal under a negative emotional valence. Changes from blue to red represent the changes from a depressed to a pleasant mood.

Furthermore, emotions can affect learning and memory processes [41]. In the same learning atmosphere, people in a good (bad) mood learn more (less) efficiently and forget more slowly (faster) [50,51]. A series of light pulses were applied to mimic the studying action of a person. The synaptic weight of the devices at 0 s after stimulation (light pulse number: 80, power density: 44.3 mW/cm^2, pulse width: 0.5 s, and pulse frequency: 1 Hz), 10 s after stimulation and 60 s after stimulation were extracted to assess the memory process. The synaptic weight is derived from the formula: $W_t = A_t/A_0 \times 100\%$, where A_0 is the ground state PSC and A_t is the amplitude of PSC at t s after learning, respectively. According to the extracted parameters, the memory process of letter 'T' at different gate voltage and time are depicted in Fig. 5c. The emotion moods are positively (negatively) related to positive (negative) gate voltages, which are consistent with the fact that learning results are positively (negatively) related to positive (negative) moods. It reveals that one has the strongest learning ability and first impressions of the letter 'T' when he/she is in a positive emotion (V_{GS} = −80 V). After a period of time, the recognition of the letter 'T' becomes blurred compared to the first impression, which is consistent with people's forgetting characteristics [52]. Finally, one with a positive emotion has a clearer impression of the letter 'T'. Therefore, the present HfS$_2$ based synaptic devices could simulate the emotion related learning and memory.

4. Conclusions

In summary, an artificial HfS$_2$ based synaptic device has been fabricated to successfully emulate the basic synaptic plasticity, such as PPF/PPD and LTP/LTD by applying a pulse laser (λ = 405 nm). It has a high responsivity of 23 A/W at the laser power density of 1.8 mW/cm^2 and an on/off ratio of about 10^5. Owing to the gate voltage dependent charge trapping effect, the photoelectronic synaptic transistor exhibits a tunable synaptic plasticity with the PPF(128%)/PPD(89%) and LTP(283%)/LTD(68%) transitions under the same wavelength of a laser pulse. The various synaptic weights and spikes stimulated metaplasticity as functions of gate voltage and light pulse frequency are used to simulate the five emotion valences and emotion related learning and memory process. In addition, thirty artificial emotional states are obtained based on the two dimensional theory of emotion (valence and arousal). This work provide an insight into the design and fabrication of 2D HfS$_2$ based synaptic devices and their applications in artificial emotional memory.

CRediT authorship contribution statement

Qiangfei Wang: Fabricated devices, Performed electrical and optoelectronic measurements, Writing original draft. **Ruiqi Jiang:** Performed electrical and optoelectronic measurements. **Zhaotan Gao:** Performed structural analysis. **Menghan Deng:** Performed structural analysis. **Junhui Chen:** Performed electrical and optoelectronic measurements. **Liangqing Zhu:** Contributed to discussions. **Liyan Shang:** Contributed to discussions. **Yawei Li:** Contributed to discussions. **Dirk**

Fuchs: Writing original draft. **Jinzhong Zhang:** Writing original draft, Supervised the research. **Zhigao Hu:** Contributed to discussions.

Declaration of competing interest

The authors declare that they have no known competing financial interests or personal relationships that could have appeared to influence the work reported in this paper.

Data availability

Data will be made available on request.

References

[1] A.E. Pereda, Electrical synapses and their functional interactions with chemical synapses, Nat. Rev. Neurosci. 15 (4) (2014) 250–263, http://dx.doi.org/10.1038/nrn3708.

[2] T.C. Südhof, Synaptic neurexin complexes: A molecular code for the logic of neural circuits, Cell 171 (4) (2017) 745–769, http://dx.doi.org/10.1016/j.cell.2017.10.024.

[3] S. Seo, B.S. Kang, J.J. Lee, H.J. Ryu, S. Kim, H. Kim, S. Oh, J. Shim, K. Heo, S. Oh, J.H. Park, Artificial van der Waals hybrid synapse and its application to acoustic pattern recognition, Nature Commun. 11 (1) (2020) 3936, http://dx.doi.org/10.1038/s41467-020-17849-3.

[4] H. Bian, Y.Y. Goh, Y. Liu, H. Ling, L. Xie, X. Liu, Stimuli-responsive memristive materials for artificial synapses and neuromorphic computing, Adv. Mater. 33 (46) (2021) 2006469, http://dx.doi.org/10.1002/adma.202006469.

[5] D. Kim, J.-S. Lee, Neurotransmitter-induced excitatory and inhibitory functions in artificial synapses, Adv. Funct. Mater. 32 (21) (2022) 2200497, http://dx.doi.org/10.1002/adfm.202200497.

[6] D. Markovic, A. Mizrahi, D. Querlioz, J. Grollier, Physics for neuromorphic computing, Nat. Rev. Phys. 2 (9) (2020) 499–510, http://dx.doi.org/10.1038/s42254-020-0208-2.

[7] B.J. Shastri, A.N. Tait, T.F. de Lima, W.H.P. Pernice, H. Bhaskaran, C.D. Wright, P.R. Prucnal, Photonics for artificial intelligence and neuromorphic computing, Nat. Photonics 15 (2) (2021) 102–114, http://dx.doi.org/10.1038/s41566-020-00754-y.

[8] C. Bartolozzi, G. Indiveri, E. Donati, Embodied neuromorphic intelligence, Nature Commun. 13 (1) (2022) 1024, http://dx.doi.org/10.1038/s41467-022-28487-2.

[9] Y. Wang, L. Yin, W. Huang, Y. Li, S. Huang, Y. Zhu, D. Yang, X. Pi, Optoelectronic synaptic devices for neuromorphic computing, Adv. Intell. Syst. 3 (1) (2020) 2000099, http://dx.doi.org/10.1002/aisy.202000099.

[10] S.O. Park, H. Jeong, J. Park, J. Bae, S. Choi, Experimental demonstration of highly reliable dynamic memristor for artificial neuron and neuromorphic computing, Nature Commun. 13 (1) (2022) 2888, http://dx.doi.org/10.1038/s41467-022-30539-6.

[11] K. He, Y. Liu, J. Yu, X. Guo, M. Wang, L. Zhang, C. Wan, T. Wang, C. Zhou, X. Chen, Artificial neural pathway based on a memristor synapse for optically mediated motion learning, ACS Nano 16 (6) (2022) 9691–9700, http://dx.doi.org/10.1021/acsnano.2c03100.

[12] S. Dai, X. Wu, D. Liu, Y. Chu, K. Wang, B. Yang, J. Huang, Light-stimulated synaptic devices utilizing interfacial effect of organic field-effect transistors, ACS Appl. Mater. Inter. 10 (25) (2018) 21472–21480, http://dx.doi.org/10.1021/acsami.8b05036.

[13] T.Y. Wang, J.L. Meng, Z.Y. He, L. Chen, H. Zhu, Q.Q. Sun, S.J. Ding, P. Zhou, D.W. Zhang, Ultralow power wearable heterosynapse with photoelectric synergistic modulation, Adv. Sci. 7 (8) (2020) 1903480, http://dx.doi.org/10.1002/advs.201903480.

[14] K.-C. Lee, M. Li, Y.-H. Chang, S.-H. Yang, C.-Y. Lin, Y.-M. Chang, F.-S. Yang, K. Watanabe, T. Taniguchi, C.-H. Ho, C.-H. Lien, S.-P. Lin, P.-W. Chiu, Y.-F. Lin, Inverse paired-pulse facilitation in neuroplasticity based on interface-boosted charge trapping layered electronics, Nano Energy 77 (2020) 105258, http://dx.doi.org/10.1016/j.nanoen.2020.105258.

[15] C. Han, X. Han, J. Han, M. He, S. Peng, C. Zhang, X. Liu, J. Gou, J. Wang, Light-stimulated synaptic transistor with high ppf feature for artificial visual perception system application, Adv. Funct. Mater. 32 (22) (2022) 2113053, http://dx.doi.org/10.1002/adfm.202113053.

[16] L. Xu, H. Xiong, Z. Fu, M. Deng, S. Wang, J. Zhang, L. Shang, K. Jiang, Y. Li, L. Zhu, L. He, Z. Hu, J. Chu, High conductance margin for efficient neuromorphic computing enabled by stacking nonvolatile van der Waals transistors, Phys. Rev. Appl. 16 (4) (2021) 044049, http://dx.doi.org/10.1103/PhysRevApplied.16.044049.

[17] C.S. Liu, H.W. Chen, S.Y. Wang, Q. Liu, Y.G. Jiang, D.W. Zhang, M. Liu, P. Zhou, Two-dimensional materials for next-generation computing technologies, Nat. Nanotechnol. 15 (7) (2020) 545–557, http://dx.doi.org/10.1038/s41565-020-0724-3.

[18] S.W. Cho, S.M. Kwon, Y.-H. Kim, S.K. Park, Recent progress in transistor-based optoelectronic synapses: From neuromorphic computing to artificial sensory system, Adv. Intell. Syst. 3 (6) (2021) 2000162, http://dx.doi.org/10.1002/aisy.202000162.

[19] H. Han, Z. Xu, K. Guo, Y. Ni, M. Ma, H. Yu, H. Wei, J. Gong, S. Zhang, W. Xu, Tunable synaptic plasticity in crystallized conjugated polymer nanowire artificial synapses, Adv. Intell. Syst. 2 (3) (2020) 1900176, http://dx.doi.org/10.1002/aisy.201900176.

[20] C.M. Tyng, H.U. Amin, M.N.M. Saad, A.S. Malik, The influences of emotion on learning and memory, Front. Psychol. 8 (2017) 1454, http://dx.doi.org/10.3389/fpsyg.2017.01454.

[21] T. Bryan, S. Mathur, K. Sullivan, The impact of positive mood on learning, Learn. Disability Q. 19 (3) (1996) 153–162, http://dx.doi.org/10.2307/1511058.

[22] H. Xiong, L. Xu, C. Gao, Q. Zhang, M. Deng, Q. Wang, J. Zhang, D. Fuchs, W. Li, A. Cui, L. Shang, K. Jiang, Z. Hu, J. Chu, Optically modulated HfS₂-based synapses for artificial vision systems, ACS Appl. Mater. Inter. 13 (42) (2021) 50132–50138, http://dx.doi.org/10.1021/acsami.1c14332.

[23] T. Kanazawa, T. Amemiya, A. Ishikawa, V. Upadhyaya, K. Tsuruta, T. Tanaka, Y. Miyamoto, Few-layer HfS₂ transistors, Sci. Rep. 6 (2016) 22277, http://dx.doi.org/10.1038/srep22277.

[24] X.R. Nie, B.Q. Sun, H. Zhu, M. Zhang, D.H. Zhao, L. Chen, Q.Q. Sun, D.W. Zhang, Impact of metal contacts on the performance of multilayer HfS₂ field-effect transistors, ACS Appl. Mater. Interfaces 9 (32) (2017) 26996–27003, http://dx.doi.org/10.1021/acsami.7b06160.

[25] K. Xu, Z. Wang, F. Wang, Y. Huang, F. Wang, L. Yin, C. Jiang, J. He, Ultrasensitive phototransistors based on few-layered HfS₂, Adv. Mater. 27 (47) (2015) 7881–7887, http://dx.doi.org/10.1002/adma.201503864.

[26] C. Gao, Q. Nie, C.-Y. Lin, F. Huang, L. Wang, W. Xia, X. Wang, Z. Hu, M. Li, H.-W. Lu, Y.-C. Lai, Y.-F. Lin, J. Chu, W. Li, Touch-modulated van der Waals heterostructure with self-writing power switch for synaptic simulation, Nano Energy 91 (2022) 106659, http://dx.doi.org/10.1016/j.nanoen.2021.106659.

[27] Q. Nie, C. Gao, F.-S. Yang, K.-C. Lee, C.-Y. Lin, X. Wang, C.-H. Ho, C.-H. Lien, S.-P. Lin, M. Li, Y.-F. Lin, W. Li, Z. Hu, J. Chu, Carrier-capture-assisted optoelectronics based on van der Waals materials to imitate medicine-acting metaplasticity, Npj 2D Mater. Appl. 5 (1) (2021) 60, http://dx.doi.org/10.1038/s41699-021-00241-0.

[28] C. Gao, M. Lee, M. Li, K. Lee, F. Yang, C. Lin, K. Watanabe, T. Taniguchi, P. Chiu, C. Lien, W. Wu, S. Lin, W. Li, Y. Lin, J. Chu, Mimic drug dosage modulation for neuroplasticity based on charge-trap layered electronics, Adv. Funct. Mater. 31 (5) (2020) 2005182, http://dx.doi.org/10.1002/adfm.202005182.

[29] B. Li, D. Yu, S.-L. Zhang, Raman spectral study of silicon nanowires, Phys. Rev. B 59 (3) (1999) 1645–1648, http://dx.doi.org/10.1103/PhysRevB.59.1645.

[30] K. Xu, Y. Huang, B. Chen, Y. Xia, W. Lei, Z. Wang, Q. Wang, F. Wang, L. Yin, J. He, Toward high-performance top-gate ultrathin HfS₂ field-effect transistors by interface engineering, Small 12 (23) (2016) 3106–3111, http://dx.doi.org/10.1002/smll.201600521.

[31] H.F. Haneef, A.M. Zeidell, O.D. Jurchescu, Charge carrier traps in organic semiconductors: A review on the underlying physics and impact on electronic devices, J. Mater. Chem. C 8 (3) (2020) 759–787, http://dx.doi.org/10.1039/c9tc05695e.

[32] Y. Park, H.W. Baac, J. Heo, G. Yoo, Thermally activated trap charges responsible for hysteresis in multilayer MoS₂ field-effect transistors, Appl. Phys. Lett. 108 (8) (2016) 083102, http://dx.doi.org/10.1063/1.4942406.

[33] A. Di Bartolomeo, L. Genovese, F. Giubileo, L. Iemmo, G. Luongo, T. Foller, M. Schleberger, Hysteresis in the transfer characteristics of MoS₂ transistors, 2D Mater. 5 (1) (2017) 015014–015019.

[34] D. Choquet, A. Triller, The dynamic synapse, Neuron 80 (3) (2013) 691–703, http://dx.doi.org/10.1016/j.neuron.2013.10.013.

[35] J. Tang, F. Yuan, X. Shen, Z. Wang, M. Rao, Y. He, Y. Sun, X. Li, W. Zhang, Y. Li, B. Gao, H. Qian, G. Bi, S. Song, J.J. Yang, H. Wu, Bridging biological and artificial neural networks with emerging neuromorphic devices: Fundamentals, progress, and challenges, Adv. Mater. 31 (49) (2019) 1902761, http://dx.doi.org/10.1002/adma.201902761.

[36] J. Zhang, S. Dai, Y. Zhao, J. Zhang, J. Huang, Recent progress in photonic synapses for neuromorphic systems, Adv. Intell. Syst. 2 (3) (2020) 1900136, http://dx.doi.org/10.1002/aisy.201900136.

[37] T. Chang, S.-H. Jo, W. Lu, Short-term memory to long-term memory transition in a nanoscale memristor, ACS Nano 5 (9) (2011) 7669–7676, http://dx.doi.org/10.1021/nn202983n.

[38] J. Murakami, R. Okada, Y. Fujito, M. Sakakibara, K. Lukowiak, E. Ito, Paired pulse ratio analysis of insulin-induced synaptic plasticity in the snail brain, J. Exp. Biol. 216 (10) (2013) 1771–1773, http://dx.doi.org/10.1242/jeb.083469.

[39] D. Kim, W.K. Min, H.T. Kim, J. Chung, M.S. Kim, H.J. Kim, Realization of enhanced long-term visual memory for indium-gallium-zinc oxide-based optical synaptic transistor, Adv. Opt. Mater. 10 (15) (2022) 2200558, http://dx.doi.org/10.1002/adom.202200558.

[40] T. Ahmed, S. Kuriakose, E.L.H. Mayes, R. Ramanathan, V. Bansal, M. Bhaskaran, S. Sriram, S. Walia, Optically stimulated artificial synapse based on layered black phosphorus, Small 15 (22) (2019) 1900966, http://dx.doi.org/10.1002/smll.201900966.

[41] E.T. Rolls, S.M. Stringer, A model of the interaction between mood and memory, Network: Comp. Neural Syst. 12 (2) (2001) 89–109, http://dx.doi.org/10.1088/0954-898X/12/2/301.

[42] Y. Wang, Y. Zhu, Y. Li, Y. Zhang, D. Yang, X. Pi, Dual-modal optoelectronic synaptic devices with versatile synaptic plasticity, Adv. Funct. Mater. 32 (1) (2021) 2107973, http://dx.doi.org/10.1002/adfm.202107973.

[43] Q. Wu, J. Wang, J. Cao, C. Lu, G. Yang, X. Shi, X. Chuai, Y. Gong, Y. Su, Y. Zhao, N. Lu, D. Geng, H. Wang, L. Li, M. Liu, Photoelectric plasticity in oxide thin film transistors with tunable synaptic functions, Adv. Electron. Mater. 4 (12) (2018) 1800556, http://dx.doi.org/10.1002/aelm.201800556.

[44] M.C. Anderson, J.C. Hulbert, Active forgetting: Adaptation of memory by prefrontal control, Annu. Rev. Psychol. 72 (1) (2021) 1–36, http://dx.doi.org/10.1146/annurev-psych-072720-094140.

[45] J.L. Andrews, S.P. Ahmed, S.J. Blakemore, Navigating the social environment in adolescence: The role of social brain development, Biol. Psychiatry 89 (2) (2021) 109–118, http://dx.doi.org/10.1016/j.biopsych.2020.09.012.

[46] A.B. Satpute, K.A. Lindquist, The default mode network's role in discrete emotion, Trends Cogn. Sci. 23 (10) (2019) 851–864, http://dx.doi.org/10.1016/j.tics.2019.07.003.

[47] L. Feldman Barrett, J. Russell, The structure of current affect: Controversies and emerging consensus, Curr. Dir. Psychol. Sci. 8 (1) (1999) 10–14, http://dx.doi.org/10.1111/1467-8721.00003.

[48] J. Wang, C. Wang, P. Cai, Y. Luo, Z. Cui, X.J. Loh, X. Chen, Artificial sense technology: Emulating and extending biological senses, ACS Nano 15 (12) (2021) 18671–18678, http://dx.doi.org/10.1021/acsnano.1c10313.

[49] X. Zhang, X. Yang, W. Zhang, G. Li, H. Yu, Crowd emotion evaluation based on fuzzy inference of arousal and valence, Neurocomputing 445 (2021) 194–205, http://dx.doi.org/10.1016/j.neucom.2021.02.047.

[50] J. Zhang, Q. Shi, R. Wang, X. Zhang, L. Li, J. Zhang, L. Tian, L. Xiong, J. Huang, Spectrum-dependent photonic synapses based on 2d imine polymers for power-efficient neuromorphic computing, Infomatics 3 (8) (2021) 904–916, http://dx.doi.org/10.1002/inf2.12198.

[51] L. Yin, W. Huang, R. Xiao, W. Peng, Y. Zhu, Y. Zhang, X. Pi, D. Yang, Optically stimulated synaptic devices based on the hybrid structure of silicon nanomembrane and perovskite, Nano Lett. 20 (5) (2020) 3378–3387, http://dx.doi.org/10.1021/acs.nanolett.0c00298.

[52] L. Sun, W. Wang, H. Yang, Recent progress in synaptic devices based on 2D materials, Adv. Intell. Syst. 2 (5) (2020) 1900167, http://dx.doi.org/10.1002/aisy.201900167.